Identification of the Constitutive and Friction Models Parameters via a Multi-Objective Surrogate-Assisted Algorithm for the Modeling of Machining-Application to Arbitrary Lagrangian Eulerian Orthogonal Cutting of Ti6Al4V

F. Ducobu, N. Kugalur-Palanisamy, G. Briffoteaux, M. Gobert, D. Tuyttens, P. Arrazola, E. Rivière-Lorphèvre

Identification of the Constitutive and Friction Models Parameters via a Multi-Objective Algorithm for the Modeling of Machining – Application to ALE orthogonal cutting of Ti6Al4V

F. Ducobu[a,*], N. Kugalur-Palanisamy[a], G. Briffoteaux[b], M. Gobert[b], D. Tuyttens[b], P.J. Arrazola[c], E. Rivière-Lorphèvre[a]

[a]*Machine Design and Production Engineering Lab, Research Institute for Science and Material Engineering, University of Mons, Belgium*
[b]*Mathematics and Operational Research Department (MARO), University of Mons, Belgium*
[c]*Mechanical and Manufacturing Department, Faculty of Engineering, Mondragon Unibertsitatea, Spain*

Abstract

The evolution of high-performance computing facilitates the simulation of manufacturing processes. The prediction accuracy of a numerical model of the cutting process is closely associated with the selection of constitutive and friction models. The reliability and the accuracy of these models highly depend on the value of the parameters involved in the definition of the cutting process. These model parameters are determined using a direct method or an inverse method. However, these identification procedures often neglect the link between the parameters of the material and the friction models. This paper introduces a novel approach to inversely identify the best parameters value for both models at the same time and by taking into account multiple cutting conditions in the optimization routine. An Artificial Intelligence (AI) framework that combines the finite

*Corresponding author.
Email address: Francois.Ducobu@umons.ac.be (F. Ducobu)

December 8, 2023

element modeling with an Adaptive Bayesian Multi-objective Evolutionary Algorithm (AB-MOEA) is developed, where the objective is to minimize the deviation between the experimental and the numerical results. The Arbitrary Lagrangian Eulerian (ALE) formulation and the Ti6Al4V alloy are selected to demonstrate its applicability. The investigation shows that the developed AI platform can identify the best parameters values with low computational time and resources. The identified parameters values predicted the cutting and feed forces within a deviation of less than 4% from the experiments for all the cutting conditions considered in this work.
Keywords: Artificial Intelligence, Multi-Objective identification, Surrogate Evolutionary Algorithm, Orthogonal cutting, Finite Element Modeling

1. Introduction

Machining is a well-known manufacturing process involving removal of material from a workpiece to achieve the desired shape and properties. For an efficient cutting process, knowledge of the forces experienced during the cutting of a material is highly significant as they influence tool wear or breakage, workpiece surface quality, etc. The forces prediction is essential to improve tool design, optimize the cutting conditions, and predict tool wear. Many analytical cutting models are developed based on maximum shear stress and minimum energy principle theories to describe the cutting mechanism [1]. The models, such as the shear plane model by Merchant et al., the slip-line field model by Lee and Shaffer, the well-known shear-zone model [2], and the variational principles of the plasticity theory due to the principle of minimum energy [3] are developed based on large numbers of assumptions. Even though these models, can be used to study the variation in tool

shape, lubrication, and material properties, their applications are limited [4].

Although experimental investigations of the cutting process may provide information, it is insufficient to model the process [5]. The experimental analysis involving mechanical and friction tests is necessary to obtain more reliable input. However, due to the limitations in the measurement technologies and experimental setups, many variables such as stresses, strain, temperature distribution, friction coefficient, etc. cannot be directly and reliably observed by experiments [6]. In addition, these experiments are highly expensive and time-consuming [5, 7, 8]. Numerical techniques are employed to overcome these difficulties [5].

The advancement in the computational field and numerical analysis enabled to develop a numerical model of the orthogonal cutting process [7, 9]. The Finite Element (FE) modeling is nowadays the most prominent numerical modeling approach established for the simulation of the metal cutting process [4]. FE simulation of the chip formation process replaces the expensive experimental tests and can predict the difficult-to-measure variables such as stress, strain, temperature, etc. with higher accuracy than an analytical model [4]. Modeling the complex machining process with a FE model is quite challenging as it involves various inputs. The efficiency of the cutting model is dependent on the numerical parameters such as formulation type (Lagrangian, Eulerian, Arbitrary Lagrangian-Eulerian, or Coupled Eulerian-Lagrangian), quality of the mesh, boundary conditions, constitutive model, contact conditions [4, 5, 7, 10–12]. However, an accurate models to describe the behavior of the material and the friction conditions between the tool and the chip during the cutting process are essential to obtain accurate and reliable results from the simulations [5, 13–15]. A reliable flow stress data that should relate the large plastic strains (1-6) at the very high strain rates (up to

10^6 s^{-1}) and the very high temperatures (800 K to 1400 K) observed during the cutting process is necessary to frame the model. In addition, the friction model should provide reliable information on the tool-chip interface.

Many distinct material models are used in numerical modeling of the machining process, and they are characterized as empirical/phenomenological, physical-based, and hybrid models [5, 10]. When compared to physical-based and hybrid models, empirical models are highly recommended for their robustness, lower number of parameters, and availability of data [5, 14] despite limitations such as the absence of a direct link with the physics. Similarly, several friction models exist that are directly related to the behavior of the material in orthogonal cutting [16, 17]. However, the credibility of the material model and the friction model is dependent on the relevant parameters involved in defining the behavior of the material throughout the machining process [18, 19].

The values of these material model parameters are obtained using either a direct method or an inverse method [10] . The direct method collects data through targeted experimental tests. The experimental approaches employ curve fitting techniques to characterize experimental data from quasi-static and dynamic material testing such as the Split Hopkinson Pressure Bar (SHPB) test. Nonetheless, these experiments can achieve a maximum strain of 0.5 and strain rate near 10^3 s^{-1},which is significantly lower than the strain of 3 or even higher, and a strain rate up to 10^6 s^{-1} that is encountered during the cutting process, necessitating data extrapolation [20, 21]. Although the pin-on-ring, pin-on-disk, open and closed tribometers [22] friction tests are available to determine the friction characteristics during the cutting process, the information is often unreliable due to events such as thermodynamical and tribological interactions existing in the cutting zone and

especially in the secondary deformation zone taking place at the tool-chip contact area [10, 15, 17, 23–25].

One of the earlier ways for determining the inverse parameter from the cutting process was published by Özel and Altan [21]. The authors' fundamental methodology is to use orthogonal cutting experiments and FEM simulations (DEFORM 2D) at the same time to identify the flow stress and friction parameters used for the range of high-speed cutting. The AISI P20 mold steel was chosen for the inverse identification technique. Only the cutting force, however, is employed to assess the connection between experimental and simulation data. In [26], the authors used Particle Swarm Optimization (PSO) to optimize the parameters of the Johnson-Cook (JC) model and the Zerilli-Armstrong model. They used an experimental database obtained from SHPB experiments in their work, which needed extrapolation into the cutting regime. In [27], the authors studied the inverse material parameter identification of the Barlat-model in the field of sheet metal forming using a Genetic approach (GA), a gradient-based approach, and a combination of both (a hybrid algorithm). According to their findings, GA and gradient-based algorithms can fit numerical values to experimental data despite the usual problems of high processing time for GA and local minima for the gradient-based technique. The authors concluded that the hybrid method performs well in identifying parameters by perhaps fitting most of the macroscopic effects.

In [28], the authors estimated the Johnson-Cook material properties of two materials, Nitronic 33 superalloy and Ti6Al4V, using a weighted multi-objective identification technique. An inverse identification strategy based on fitting the model to the experimental data is considered. The recommended strategy was found to be admirable in terms of decreasing the number of experiments required.

In [29], the authors used an inverse technique to determine the JC material and damage parameters for AISI 316L stainless steel. Lower and upper values that underestimated and overestimated the experimental results were guessed to define the model parameters, and the material model parameters were interpolated to obtain the best fit with the experimental data. In their approach, the parameters A, B, and n are approximated by the least squares method and held constant throughout their approach, whereas the parameters C and m are calculated. Later, the same approach was used in [29] to obtain the material model parameters of AISI 1045 and Inconel 718. According to the authors, the measured and predicted cutting forces, chip geometries, and temperatures are quite near. However, numerous downsides are identified, such as the chance that a unique solution is not always provided, because various parameter combinations can result in the same simulation results for the analyzed conditions. Furthermore, the method can be trapped in a local minimum [30].

In [31], the authors utilized PSO in conjunction with Oxley's machining theory to determine constitutive parameters of the JC flow stress model by inverse modeling in combination with an approach to predict forces and temperatures for the material 70MnVS4 and a novel aluminum-alloyed UHC-steel. The main drawbacks resulting from the assumptions and simplifications of Oxley's machining theory determine this approach [32]. In [33, 34], the authors used an inverse approach to re-identify only two parameters, A and B from the JC material model consisting of 5 parameters. The Levenberg-Marquardt optimization algorithm was used by the authors to inversely determine the parameters set. In this approach, a FE simulation was performed with a known set of parameters for a particular cutting condition, and the parameters were re-identified independently by com-

paring the chip morphology and the cutting force. In [35], the authors compared the Downhill-Simplex-Algorithm, the GA, and a hybrid method to determine the five JC parameters of AISI 304 stainless steel and the Tresca friction parameter. The objective function was expressed as the weighted sum of the relative errors in the estimation of the cutting force, the chip thickness, and the chip curvature. The authors claimed that with the proposed hybrid algorithm, it is possible to determine the parameters after 115 simulations. However, despite a large number of simulations, the results revealed solely an agreement between the simulated and experimental data, with deviations up to 113 %. In this work, only one cutting condition was investigated, so validity is expected to be limited.

In [36], the authors developed an inverse optimization methodology to determine the JC material model parameters of AISI 316L and SAF 2507 super-duplex stainless steel. The routine was developed in a Dassault Systemes ISight environment. AdvantEdge was employed to simulate the 2D orthogonal cutting process. An optimization algorithm was utilized to identify the JC parameters (A, B, C, n, and m) and the best Coulomb's friction coefficients for the cutting conditions. The authors used a sequential procedure with a specific design of computer experiments, and Radial Basis Functions to generate the regression models based on forces and temperatures for the optimization problem. Subsequently, a Multi-Island GA was used to identify the best collection of JC material model parameters by minimizing an objective function. The authors mentioned that the identified JC parameters values and Coulomb's friction coefficients can reduce the maximum deviation to less than 15 % for cutting force and temperatures, but a higher maximum deviation was observed in terms of feed force (higher than 60 %). In addition, the characteristics of the chip (i.e. its geometry) were not taken into

account.

In [37, 38], the authors proposed an approach based on the Downhill-Simplex algorithm for the inverse identification of JC material parameters from FE simulations. The authors applied a multi-objective optimization approach to AISI 1045 steel and claimed that it is possible to re-identify two parameters within a small number of iterations. However, the authors focused on the re-identification of the two model parameters that have a rather small influence on the flow stress, as opposed to the exponential model parameters. In [39], the authors further tested the approach presented in [38]. They performed simulations with an initial parameters set (A, B, C, m, n) acquired from the literature, to simulate the orthogonal cutting process. The main drawback was that the quantities of interest found from the numerical simulation were used as an error function to inversely re-identify parameters values. Besides, the algorithm may get trapped in local minima. In [40], the authors employed PSO instead of the Downhill-Simplex-Algorithm to inversely re-determine material model parameters from orthogonal cutting simulations of AISI 1045 steel. The major investigation focused on the application and performance of the PSO algorithm. The authors concluded that the PSO algorithm identifies the parameters in a few iterations when compared to an earlier work [39]. However, the authors neglected the influence of the friction parameters and lagged in justifying the values of the weighted factors as they were chosen arbitrarily. In [41], the authors extended their work by increasing the number of quantities of interest in the objective function in addition to post-processing automation. The authors highlighted that the identification is sensitive to the initial parameters set and also highlighted the non-uniqueness of the parameters of the JC material model.

Most inverse identification approaches in the literature lag in taking into account the link between the parameters of the constitutive model and the friction model. Many algorithms developed for the identification of parameters values of constitutive models based on local search or the classical global algorithms, such as GA and PSO, take weeks or even months to find the optimal values of the parameters. Furthermore, the absence of complete automation may lead to human errors and require more time and effort to transfer data. In [42], the authors identified the JC and Coulombs models' parameters as correlative by implementing a surrogate-based Efficient Global Optimization algorithm. The authors concluded that the developed AI framework is highly significant and efficient, as the optimization algorithm along with the developed FE model identifies the best parameters set within 300 iterations with a total computational time of 8 days (without parallel computing). The identified parameters set predicts the forces within a total deviation of less than 10% for the considered cutting condition. Although this is close to the experimental dispersion, there is room for improvement as a single cutting condition was considered in that optimization. Once again, the non-uniqueness of the solution has been highlighted, and then confirmed for another FE formulation [43].

In this paper, the previously introduced AI framework for the inverse identification of both the JC constitutive and Coulomb's friction models is further developed and extended to consider to more realistic and accurate case of multiple cutting conditions. A finite element model with Arbitrary Lagrangian-Eulerian formulations (ALE) for the orthogonal cutting process is considered as the simulator. A surrogate-based Adaptive Bayesian Multi-Objective Evolutionary Algorithm (AB-MOEA), which tackles the problem as a real multi-objective one, is

implemented. Three different cutting conditions with varying uncut chip thickness, h = 0.1, 0.06 and 0.04 mm, and fixed cutting speed (of 30 m/min) that produce a continuous chip during orthogonal cutting experiments are considered for the inverse identification problem.

This work brings the novelty of identifying the parameters values of the constitutive model and friction model together by considering multiple cutting conditions in the optimization routine. In addition, two different optimization formulations are investigated:

- Three-objective functions for the three considered cutting conditions. Each objective function is defined based on minimizing the deviation of the FE numerical simulation outcomes to the experimental outcomes with a weighted average defined over the quantities of interest.

- Nine-objective functions for the three cutting conditions. Each objective function is defined based on minimizing the deviation of the numerical simulation outcome to the experimental outcome for one quantity of interest.

The paper is organized as follows. The material constitutive and friction models selected for this particular work, JC and Coulomb, respectively, are presented in Section 2. The experimental references and the developed Arbitrary Lagrangian-Eulerian Finite Element model implemented for the simulation of orthogonal cutting are presented in Section 3. The fourth section delves into the adopted specific methodologies, introducing and explaining the two formulations of the multi-objective optimization problem. The surrogate-based optimization algorithm employed in this study is presented in Section 5. The numerical experiments and the obtained results are presented and discussed in Section 6. Finally, Section

7 wraps up the article with a conclusion that summarizes the key findings and suggests directions for future research.

2. Constitutive and Friction Models

The accuracy of a FE model depends on various inputs. The two main important are the material constitutive model and the friction model. The material constitutive model describes the behavior of the material under various conditions. The parameters of this model define how the material responds to cutting. The friction model, on the other hand, deals with the contact interactions. The parameters of this model define the frictional forces at the contact interface.

This section discusses the selected constitutive and friction models, their parameters, and the relevance of optimization routines for the determination of these parameters.

2.1. Constitutive Model

Orthogonal cutting modeling involves a complex thermo-mechanical coupled material behavior that relates the flow stress to strain, strain rate, and temperature. A constitutive model describes and relates the high strain, strain rate and temperature to the flow stress response of metals during the machining process. Its general form is given in Equation 1:

$$\sigma = \sigma(\varepsilon, \dot{\varepsilon}, T) \tag{1}$$

Many constitutive models have been developed and proposed for FE modeling of the orthogonal cutting process based on real industrial machining applications. Empirical models are considered for their flexibility in adapting to various materials [10, 17]. The JC constitutive model [44] is one of the most widely employed

material models relating the strain, the strain rate, and the temperature under machining conditions. The large availability of data, its mathematical simplicity, and its low computational time and memory requirements led to wide exploitation of the model in the simulation of the machining process.

The JC flow stress equation is expressed by combining the plastic term, the viscous term, and the thermal softening term:

$$\sigma = (A + B\varepsilon^{n})\left[1 + Cln\left(\frac{\dot{\varepsilon}}{\dot{\varepsilon}_0}\right)\right]\left[1 - \left(\frac{T - T_{room}}{T_{melt} - T_{room}}\right)^{m}\right] \quad (2)$$

The JC equation is governed by the five material parameters (A, B, C, m, n) and their values depend on the material subjected to the cutting process. The yield stress of the material at the reference (room) temperature gives the value of parameter A, the modulus of strain hardening is parameter B, the strain hardening exponent is n, the strain rate sensitivity is C, and the thermal softening exponent is m. T is the current temperature, T_{melt} and T_{room} are the melting and room temperatures, respectively, while $\dot{\varepsilon}_0$ is the reference strain rate (usually fixed at 1 s^{-1}).

Identifying the values of the parameters is still a major concern for the successful simulation of the Ti6Al4V alloy orthogonal cutting process. Many other material models have been developed by modifying the JC model to represent the unique behavior of Ti6Al4V alloy [10]. For example, in [45], the authors incorporate strain-softening terms into the JC model to predict the segmented chip in the orthogonal cutting simulation of Ti6Al4V alloy. While in [46], some modifications are introduced in the previous model to better control the thermal softening effect. However, those models involve more parameters, and these parameters are determined by fitting a curve between the measured and the predicted results from orthogonal cutting tests without considering the material characterization. Nevertheless, thanks to its limited number of parameters, and the wide availability

and applications of the JC model, it was selected for this work. It is important to highlight that the novel method for inverse identification of parameters values of the JC model presented in this paper is applicable to any material model.

2.2. Friction Model

The simulation results of the orthogonal cutting model, in addition to the material model, are highly influenced by the friction conditions [15]. Along with the material model and its parameters, another key issue that must be considered for successful simulations is the friction model coefficient between the tool and the chip [5, 10, 47]. In [10], the authors carried out significant research on the impact of friction conditions in simulating the cutting process.

Coulomb's (or sliding) friction model is adopted in this work to define the friction conditions at the tool and chip interface. According to the classic Coulomb's friction model, the frictional sliding force is proportional to the applied normal load. The coefficient of friction, μ, is defined as the frictional sliding force divided by the applied normal force. The coefficient of friction remains constant during the along contact length between chip and tool. Coulomb's friction law is given in Equation 3:

$$\tau = \mu\sigma \tag{3}$$

Even though it has been criticized by the researchers, Coulomb's model is still extensively employed for its simple mathematical expression and the good qualitative trends it provides in the absence of a better accepted alternative [10, 17, 24]. Based on that observation, Coulomb's friction model is chosen in this study.

To determine the value of this coefficient during the cutting process, friction tests are conducted. However, the result is inadequate and uncertain due to com-

plex phenomena taking place at the tool-chip contact area [10, 23]. This motivates the use of an inverse identification procedure. In [15], authors justify the importance of optimizing the friction coefficient value in correlation with the material model parameter value to have a better prediction on the quantities of interest through orthogonal cutting simulation.

3. Finite Element Orthogonal Cutting Model

This section discusses the construction of the FE orthogonal cutting model of Ti6Al4V, as well as the automation procedure required to assist the optimization process. The ALE model, dedicated to the production of continuous chips with initial chip geometry, to develop a FE predictive model for the cutting process will be presented. The automation script set up to manage the output file created by the Abaqus FE program following a successful simulation of the machining process is described.

3.1. Arbitrary Lagrangian-Eulerian FE model

In FE modeling, the Eulerian and the Lagrangian formulations are usually considered [4, 5]. The computational mesh is fixed in the Eulerian technique, while the material moves, allowing for substantial material deformation. Prior information on the chip geometry is required to model the machining simulations with the Eulerian formulation [5] and it is adopted only for steady state chip formation. In the Lagrangian formulation, the nodes of the mesh are attached to the material and follow the material's deformation. It induces large mesh distortions and frequent remeshing operations are needed to deal with large material deformations. In addition, without remeshing, the Lagrangian formulation needs chip separation criteria [4, 48].

The Arbitrary Lagrangian-Eulerian (ALE) and the Coupled Eulerian-Lagrangian (CEL) formulations were developed to overcome the drawbacks of the Eulerian and Lagrangian formulations. In the Eulerian ALE formulation, the material flows through the mesh similarly to the Eulerian formulation. Because of this freedom in movement of the mesh, the ALE description can accommodate high distortions with more resolution [49]. In the CEL formulation, a Lagrangian part is modeled within a Eulerian domain and the efficiency of the model depends on the Eulerian mesh definition; no mesh distortion occurs [11].

In this work, an explicit Eulerian ALE finite element formulation is adopted to simulate the orthogonal cutting process of Ti6Al4V. This ALE formulation combines the advantages of Lagrangian and Eulerian, allowing for the consideration of significant deformations during material flow around the tool's cutting edge without the use of a chip separation criterion. Eulerian boundary conditions with adaptive constraints are defined on the workpiece inflow (left), outflow (right), and chip outflow (see Figure 1). The FE software Abaqus 6.14 is used to model the thermo-mechanical chip formation process.

In this FE model, a two-dimensional (2D) plane strain configuration is considered as 2D models are computationally less expensive, simpler, and easier to implement than 3D models; this can be significantly advantageous in an optimization loop. It is important to stress that the presented AI identification method can be used with any FE formulation and any dimensionality. The tool is fixed, and the workpiece moves at the prescribed cutting speed of 30 m/min. The length of the workpiece is $4h \times 1.5$ where h is the uncut chip thickness and $4h$ is the initial width of the workpiece. The initial geometry of the chip is predefined with respect to h. The initial geometry and the boundary conditions are illustrated in Figure 1.

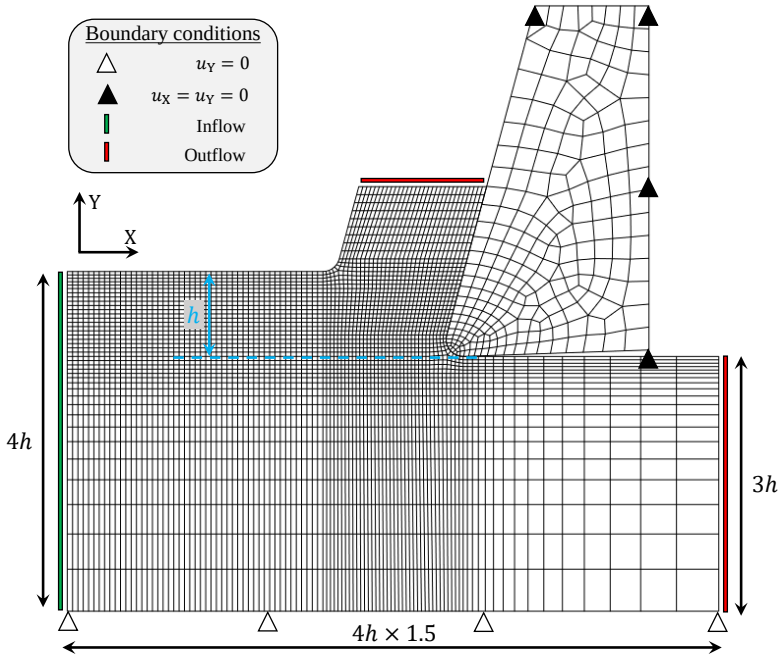

Figure 1: ALE model with initial geometry, initial mesh structure and boundary conditions representing Eulerian boundary in the inflow and outflow regions

The tool and the workpiece are meshed using quadrilateral elements with reduced integration (CPE4RT). The area near the cutting zone (near the tool-tip) is modeled with a finer mesh of size 5 μm $\times$ 5 μm according to a previous mesh sensitivity study [50]. The stable time increment of the simulations has been artificially increased using the mass scaling technique. Given that it resulted in a large reduction in calculation time without compromising the results, a mass scaling factor of 1,000 was taken into consideration [51]. This technique is essential for achieving the steady state for force calculations with a reasonable computing time (42 min on 6 cores of an Intel i7-10700 CPU @2.90 GHz with 16 GiB of Ram).

The tool material is tungsten carbide, and it is assumed to have a linear elastic

behavior. The material properties adopted in the model are given in Table 1. The thermal properties are adopted from the literature [52]. The initial temperature for tool and workpiece is set to 298 K. The tool geometry and the cutting conditions are given in Table 2.

Table 1: Material properties considered for this study [52, 53]

Material properties	Ti6Al4V	Tungsten Carbide
Young's modulus (GPa)	113.8	800
Density (kg/m^3)	4430	15000
Poisson's ratio	0.342	0.2
Expansion (K^{-1})	8.6E-6	4.7E-6
Conductivity (W/mK)	7.3	46
Specific heat (J/kgK)	580	203
Convection (W/m^{2}K)	50	
Radiation	0.3	

Table 2: Cutting and tool parameters

Cutting and Tool Parameters	Values
Cutting speed (m/min)	30
Uncut chip thicknesses (mm)	0.1, 0.06, 0.04
Rake angle (°)	15
Clearance angle (°)	2
Cutting edge radius (mm)	0.02

3.2. Post processing automation

A script for post-processing automation has been written. After processing the input file and completing the computation, it investigates the output file (.ODB in Abaqus) saved in a designated folder. The information from the specific nodes is accessed. Then, the Root Mean Square (RMS) calculations of forces are performed and euclidean distance between the chip sides is calculated to obtain the desired results: the cutting force, the feed force and the chip thickness.

The cutting and feed forces are evaluated by considering the RMS value at the steady state. The information on the coordinate points of the chip is required to calculate the chip thickness. The chip produced by the simulation is continuous and its sides have therefore the shape of a curve. This prevents direct measurement of the chip thickness. To achieve it, both sides of the chip are modeled with Bézier curves, and the chip thickness is measured as an average of the distance between those curves evaluated at several points. In addition, kinetic energy and internal energy information is acquired to check the stability of the ALE model with mass scaling [51]. The post-processing script helps analyzing the results faster and more accurately in an automatic way.

4. Multi-Objective Optimization problems

The problem of identifying the model parameters value considers the JC model parameters (B, C, n, m) and the Coulomb's friction parameter μ. The parameter value A, which is the yield stress value of the Ti6Al4V in the JC model, is set to 997.9 MPa [53, 54] in order to be in accordance with the mechanical characteristics of the material. Consequently, a candidate solution for the optimization problem is represented by the following decision vector:

$$\boldsymbol{x} = \begin{pmatrix} B & C & m & n & \mu \end{pmatrix} \in \mathbb{R}^5 \tag{4}$$

The ranges for the decision variables are presented in Table 3 and are set according to [12]. In [12], the authors investigated 20 sets of JC model parameters available in the literature for the Ti6Al4V alloy. The bounds for the friction coefficient are $\mu \in [0, 1]$.

Table 3: Ranges of the decision variables

Parameter	Lower bound	Upper bound
B (MPa)	331.2	1092
C	0.000022	0.05
m	0.6437	1.51
n	0.122	1.01
μ	0	1

In this study, we propose two formulations of the parameters identification problem. The first formulation minimizes a 3-objective function, $\boldsymbol{f}(\boldsymbol{x})$, while the second one minimizes a 9-objective function, $\boldsymbol{g}(\boldsymbol{x})$. Both objective functions $\boldsymbol{f}$ and $\boldsymbol{g}$ rely on three quantities of interest summarized in Table 4. Each quantity of interest has previously been evaluated by physical experiments ($y_{j,phy}$). Given a set of parameters value $\boldsymbol{x}$, the FE model can approximate every quantity of interest by numerical experiments ($y_{j,num}$). The main goal is to find the decision vector $\boldsymbol{x}$ that best fits the numerical outcomes to the physical ones. In the following, the dependence to $\boldsymbol{x}$ is sometimes omitted for readability purpose.

The 3-objective function $\boldsymbol{f}$ is described in Equation 5:

Table 4: Quantities of interest

Variable name	Quantity of interest	Unit
y_1	cutting force F_c	N/mm
y_2	feed force F_f	N/mm
y_3	chip thickness h'	mm

$$\begin{aligned} \boldsymbol{f} &= \left(f^{(1)}, f^{(2)}, f^{(3)}\right) \in [0,1]^3 \\ f^{(i)}(\boldsymbol{x}) &= \frac{1}{3}\sum_{j=1}^{3} \frac{|y^{(i)}_{j,num}(\boldsymbol{x}) - y^{(i)}_{j,phy}|}{max|y^{(i)}_{j,num}(\boldsymbol{x}) - y^{(i)}_{j,phy}|} \end{aligned} \tag{5}$$

Each component $f^{(i)}$ represents the weighted average of the absolute difference between numerical (*num*) and physical (*phy*) experiments for the three quantities of interests under a particular cutting condition i. Every absolute difference is normalized by the maximum possible value. The weights are chosen uniformly in order to give the same importance to every quantity of interest and to every cutting condition. As a result, $f^{(i)}$ outputs values in the range $[0, 1]$.

Table 5 lists the three cutting conditions that were taken into account for parameter identification and are defined by a specific value for the uncut chip thickness h. The remaining parameters listed in Table 2 are all kept constant.

Table 5: Cutting conditions considered for parameters identification (cutting speed is constant at 30 m/min, see Table 2 for other cutting parameters)

Cutting condition index	Uncut chip thickness h (mm)
1	0.04
2	0.06
3	0.1

The 9-objective function $\boldsymbol{g}$ is described in Equation 6:

$$\begin{aligned} \boldsymbol{g} &= \left(g_1^{(1)}, g_2^{(1)}, g_3^{(1)}, g_1^{(2)}, g_2^{(2)}, g_3^{(2)}, g_1^{(3)}, g_2^{(3)}, g_3^{(3)}\right) \\ g_j^{(i)}(\boldsymbol{x}) &= \frac{|y_{j,num}^{(i)}(\boldsymbol{x}) - y_{j,phy}^{(i)}|}{max|y_{j,num}^{(i)}(\boldsymbol{x}) - y_{j,phy}^{(i)}|} \in [0,1] \end{aligned} \tag{6}$$

Each component $g_j^{(i)}$ represents the normalized difference between numerical (*num*) and physical (*phy*) experiments for the quantity of interest j under the cutting condition i. In the following, the optimization problem consisting of minimizing $\boldsymbol{f}$ (respectively $\boldsymbol{g}$) is referred to as 3Obj-3C (respectively 9Obj-3C).

5. Surrogate-based Multi-Objective Evolutionary Algorithms

Multi-objective Evolutionary Algorithms (MOEAs) are well-known optimization algorithms to address black-box multi-objective problems [55]. Black-box problems are characterized by a lack of information about the mathematical properties of the objective function as in the identification of the JC and friction model parameters. To perform well, MOEAs require a high number of evaluations of the objective function which is an important drawback when these evaluations are computationally expensive as it is the case in this study.

To overcome this drawback, surrogate models are deployed to save computational effort by predicting the outcomes of the real objective function in a fast way. A surrogate-model approximates the behavior of a complicated and expensive simulation model while being computationally less expensive to analyze. Surrogate models are beneficial as they reduce the number of simulations needed to identify the optimal solution. The AB-MOEA [56] is a surrogate-driven algorithm which consists in adequately acquiring new sets of model parameters to be evaluated with the real objective function. The acquisition function relies on the prediction and on the predictive uncertainty provided by the surrogate-model. Minimizing the predicted objective vectors $\hat{\boldsymbol{f}}$ favors exploitation of the space of model parameters while maximizing the predictive uncertainty $\hat{\boldsymbol{s}}^{\mathbf{2}}$ promotes exploration. The AB-MOEA is composed of a surrogate-free MOEA (the Reference Vector guided Evolutionary Algorithm, RVEA), an adaptive acquisition function ($\boldsymbol{f_{ada}}$) based on a surrogate-model and an adaptive sampling criterion. These components are detailed in the next sub-sections.

5.1. Reference Vector guided Evolutionary Algorithm

The Reference Vector guided Evolutionary Algorithm (RVEA) has been recently proposed in [57] to address many-objective optimization problems (problems with three objectives and more). The main complexity in multi- and many-objective optimization is to balance convergence and diversity in the objective space. Two ingredients are proposed in [57] to balance convergence and diversity. On the one hand, a set of reference vectors is introduced in order to decompose the objective space, and on the other hand, a new distance, termed angle penalized distance, is introduced to adaptively regulate the balance during the search.

The general structure of RVEA, which is presented in Algorithm 1, is roughly

the same as that of a traditional evolutionary algorithm [58]. The novelty in the algorithm structure is the initialization and the update of the reference vectors (line 1 and 11 respectively) and the replacement step (line 9).

Initialization

The main goal of the set of reference vectors is to enhance diversity by uniformly decomposing the objective space into sub-populations. Each reference vector is representative of one sub-population and each new candidate solution is affected to the sub-population whose representative reference vector is the closest. Consequently, the initial set of reference vectors must cover the objective space uniformly. To reach this characteristic, it is proposed to generate unit reference vectors $\boldsymbol{v_{1,j}}$ in the first quadrant through the simplex-lattice method [59] (line 1 in Algorithm 1). Firstly, n_{ref} m-dimensional vectors $\boldsymbol{u_j} = \left(u_j^1, \ldots, u_j^m\right)$ for $j \in \{1, \ldots, n_{ref}\}$ are generated according to Equation 7:

$$\begin{cases} \sum_{k=1}^{m} u_j^k = 1 \ \forall j \in \{1, \ldots, n_{ref}\} \\ u_j^k \in \left\{\frac{0}{s_l}, \frac{1}{s_l}, \ldots, \frac{s_l}{s_l}\right\} \ \forall (j,k) \in \{1, \ldots, n_{ref}\} \times \{1, \ldots, m\} \end{cases} \tag{7}$$

where $s_l \in \mathbb{N}^+$ determines the number of reference vectors through the following formula:

$$n_{ref} = \begin{pmatrix} s_l + m - 1 \\ m - 1 \end{pmatrix} \tag{8}$$

with m representing the number of objectives. Secondly, the reference vectors $\boldsymbol{v_{1,j}}$ are set according to Equation 9:

$$\boldsymbol{v_{1,j}} = \frac{\boldsymbol{u_j}}{||\boldsymbol{u_j}||} \tag{9}$$

Selection and reproduction

The selection of parents consists in sampling randomly $\lfloor \frac{n_{ref}}{2} \rfloor$ pairs of parents from

Algorithm 1 Reference Vector guided Evolutionary Algorithm

Input

$\boldsymbol{f}$: real objective function

n_{ref}: number of reference vectors

n_{gen}: maximum number of generations

f_{upd}: frequency of update

$\mathcal{V}_1 \leftarrow$ simplex_lattice(n_{ref}) ▷ initial set of reference vectors

$\mathcal{P}_1 \leftarrow$ initial_sampling(n_{ref})

evaluation($\mathcal{P}_1$, $\boldsymbol{f}$)

for $i = 1 : n_{gen}$ **do**

    $\mathcal{P}_i^{par} \leftarrow$ select_parents($\mathcal{P}_i$)

    $\mathcal{P}_i^{chld} \leftarrow$ reproduction($\mathcal{P}_i^{par}$)

    evaluation($\mathcal{P}_i^{chld}$, $\boldsymbol{f}$)

    $\mathcal{P}_i \leftarrow \mathcal{P}_i \cup \mathcal{P}_i^{chld}$

    $\mathcal{P}_{i+1} \leftarrow$ reference_vector_guided_replacement(i, $\mathcal{P}_i$, $\mathcal{V}_i$)

    if $i \bmod \lfloor n_{gen} \cdot f_{upd} \rfloor == 0$ **then**

        $\mathcal{V}_{i+1} \leftarrow$ reference_vector_update(i, $\mathcal{P}_{i+1}$, $\mathcal{V}_i$, $\mathcal{V}_1$)

    else

        $\mathcal{V}_{i+1} \leftarrow \mathcal{V}_i$

    end if

end for

return best Non-Dominated Front from $\mathcal{P}_{n_{gen}+1}$

the current population (line 5). Each pair of parents is mated through SBX crossover and polynomial mutation [58] (line 6) to generate a population of children.

Reference Vector guided replacement

The replacement step (line 9) is composed of three sub-steps. Firstly, the objective vectors from the population $\mathcal{P}_i$ are translated to fit in the first quadrant in the objective space. Secondly, the population is divided into sub-populations based on the distance to the reference vectors. Thirdly, one individual per sub-population is kept to form the new population $\mathcal{P}_{i+1}$.

The objective vector translation is realized thanks to the following formula:

$$\boldsymbol{y'_{i,l}} = \boldsymbol{y_{i,l}} - \boldsymbol{z_i^{min}} \text{ for } l \in \{1, \ldots, |\mathcal{P}_i|\} \tag{10}$$

where $\boldsymbol{y_{i,l}}$ is the objective vector associated to $\boldsymbol{x_{i,l}}$ (the l-th individual from $\mathcal{P}_i$) and $\boldsymbol{z_i^{min}} = \begin{pmatrix} z_{i,1}^{min} & \ldots & z_{i,m}^{min} \end{pmatrix}$ is the vector containing the minimum values known so far for each objective. $\boldsymbol{z_i^{min}}$ is also called the ideal point and the purpose of the translation is to move the objective vectors to the first quadrant where the ideal point is the origin.

Subsequently, the population $\mathcal{P}_i$ is divided into n_{ref} sub-populations $\mathcal{P}_{i,1}, \ldots, \mathcal{P}_{i,n_{ref}}$ where the representative of sub-population $\mathcal{P}_{i,j}$ is the reference vector $\boldsymbol{v_{i,j}}$. Determining the closest reference vector to a given translated objective vector $\boldsymbol{y'_{i,l}}$ amounts to determining the sub-population the individual $\boldsymbol{x_{i,l}}$ belongs to. The acute angle between the reference vectors and the objective vector is a distance measure as a small angle value reflects a close proximity: $\mathcal{P}_{i,j^*} = \{\boldsymbol{x_{i,l}} | j^* = argmax_{j \in \{1,\ldots,n_{ref}\}} \cos\theta_{i,l,j}\}$ where, $\cos\theta_{i,l,j} = \frac{\boldsymbol{y'_{i,l}} \cdot \boldsymbol{v_{i,j}}}{||\boldsymbol{y'_{i,l}}||}$.

Finally, for each sub-population, the individual minimizing the angle penalized distance is retained to be part of the new population. The angle penalized

distance is given by

$$d_{i,l,j} = (1 + P(\theta_{i,l,j})) \cdot \|\boldsymbol{y'_{i,l}}\| \tag{11}$$

where

$$P(\theta_{i,l,j}) = m \cdot \left(\frac{i}{n_{gen}}\right)^2 \cdot \frac{\theta_{i,l,j}}{\gamma_{\boldsymbol{v_{i,j}}}} \tag{12}$$

where $\gamma_{\boldsymbol{v_{i,j}}}$ is the smallest angle value between reference vector $\boldsymbol{v_{i,j}}$ and the other reference vectors in $\mathcal{V}_i$.

At the beginning of the search $\frac{i}{n_{gen}}$ is small thus $d_{i,l,j} \approx \|\boldsymbol{y'_{i,l}}\|$. So, the angle penalized distance favors convergence since a small value for $\|\boldsymbol{y'_{i,l}}\|$ amounts for an objective vector $\boldsymbol{y_{i,l}}$ close to the ideal point. However, as the search proceeds, more importance is given to the term $\frac{\theta_{i,l,j}}{\gamma_{\boldsymbol{v_{i,j}}}}$ that is as small as $\boldsymbol{y'_{i,l}}$ is close to $\boldsymbol{v_{i,j}}$, thus indicating a better diversity. From the angle penalized distance definition, diversity is said to be good when the translated objective vectors are close to their associated reference vectors.

It is worth noting that the population size may vary during the search because a sub-population may be empty.

Reference Vector update

The last step of a RVEA iteration resides in updating the reference vectors (line 11 in Algorithm 1). This step ensures obtaining a uniformly distributed Non-Dominated Front (NDF) even for problems where the different objectives are scaled to different ranges. The update is realized according to the following formula:

$$\boldsymbol{v_{i+1,j}} = \frac{\boldsymbol{v_{1,j}} \odot (\boldsymbol{z^{max}_{i+1}} - \boldsymbol{z^{min}_{i+1}})}{\|\boldsymbol{v_{1,j}} \odot (\boldsymbol{z^{max}_{i+1}} - \boldsymbol{z^{min}_{i+1}})\|} \text{ for } j \in \{1, \ldots, n_{ref}\} \tag{13}$$

where $\boldsymbol{z^{max}_{i+1}}$ (resp. $\boldsymbol{z^{min}_{i+1}}$) is the vector made of the maximum (resp. minimum)

objective values at the $i+1$ generation and $\odot$ is the element-wise product. The reference vector update should only be performed once in a while to ensure a stable convergence. The frequency of update f_{upd} is set to 0.1 as in [57]. The complexity of RVEA is $O(m \cdot n_{ref}^2)$.

5.2. Adaptive Bayesian Multi-Objective Evolutionary Algorithm (AB-MOEA)

The AB-MOEA, described in Algorithm 2, is made of three steps. The first step consists in proposing a set of new candidates by minimizing the predicted objective vectors thanks to RVEA (line 5). As no predictive uncertainty is used, only exploitation is favored. The second step consists in re-evaluating the last population returned by RVEA thanks to an adaptive function $\boldsymbol{f_{ada}}$ (line 8) defined by

$$\boldsymbol{f_{ada}}(\boldsymbol{x}, \alpha) = (1-\alpha)\hat{\boldsymbol{f}}(\boldsymbol{x})./\hat{\boldsymbol{f}}_{\boldsymbol{max}} + \alpha\hat{\boldsymbol{s}}^{\boldsymbol{2}}(\boldsymbol{x})./\hat{\boldsymbol{s}}^{\boldsymbol{2}}_{\boldsymbol{max}} \tag{14}$$

where

$$\alpha = -0.5\cos\left(\frac{b_c}{b}\pi\right) + 0.5 \tag{15}$$

where $\frac{b_c}{b}$ is the proportion of the budget already spent, ./ is the element-wise division, $\hat{\boldsymbol{f}}_{\boldsymbol{max}}$ is the per-objective maximum predicted objective vector observed in the last population returned by RVEA and $\hat{\boldsymbol{s}}^{\boldsymbol{2}}_{\boldsymbol{max}}$ is the per-objective maximum predictive variance.

At the beginning of the search ($\alpha \approx 0$), $\boldsymbol{f_{ada}}$ favors convergence to the true Pareto front by minimizing the predicted objective vectors. As the search proceeds, α increases and so minimization of the predictive variance is included to reinforce exploitation. In the third step, q candidates are retained for computationally expensive evaluation based on an adaptive sampling criterion described in Algorithm 3.

Algorithm 2 AB-MOEA

Input

$\boldsymbol{f}$: real objective function

m: number of objectives

surrogate: surrogate model

budget: budget for the search

q: number of real evaluations per cycle

database ← initial_sampling($\boldsymbol{f}$)
surrogate ← training(*database*)
$b_c \leftarrow 0$
while b_c <*budget* **do**
    $(\mathcal{B}, \mathcal{V})$ ← RVEA($\boldsymbol{f}$, 105, 20, 0.1) ▷ last population and reference vector set from Algorithm 1
    update(b_c)
    $\alpha \leftarrow -0.5 \cos\left(\frac{b_c}{budget}\pi\right) + 0.5$
    evaluate($\mathcal{B}$, $\boldsymbol{f_{ada}}$, α)
    $\mathcal{B}_{sim}$ ← adaptive_sampling_criterion($\mathcal{B}$, $\mathcal{V}$, α, q, m, b_c, *budget*)
    evaluation($\boldsymbol{f}$, $\mathcal{B}_{sim}$)
    database ← *database* $\cup\mathcal{B}_{sim}$
    surrogate ← training(*database*)
end while
return best NDF from *database*

Algorithm 3 Adaptive Sampling Criterion in AB-MOEA

Input

$\mathcal{B}$: set of candidates

$\mathcal{V}$: set of reference vectors

α: adaptive parameter

q: number of candidates to retain

m: number of objectives

b_c: budget already spent

budget: total budget

for $i = 1 : |\mathcal{B}|$ **do**
  $\boldsymbol{y}'_i \leftarrow \text{translate}(\boldsymbol{y}_i)$
  $j \leftarrow \text{sub\_population\_index}(\mathcal{V}, \boldsymbol{y}'_i)$
  if $\alpha < 0.5$ **then**
    $d_i \leftarrow m\frac{\theta(\boldsymbol{y}'_i, \boldsymbol{v}_j)}{\gamma_{\boldsymbol{v}_j}}$
  else
    $d_i \leftarrow (1 + P(\theta(\boldsymbol{y}'_i, \boldsymbol{v}_j), m, b_c, budget)) \cdot \|\boldsymbol{y}'_i\|$
  end if
end for
$\mathcal{B} \leftarrow \text{sort\_per\_sub\_population}(\boldsymbol{d}, \mathcal{B})$
return q first candidates from $\mathcal{B}$

The sampling criterion is similar to the reference vector guided replacement of RVEA. First, the predicted objective vectors are translated according to Equation (10) (line 2). Then, for each predicted objective vector, an angle-based distance from the closest reference vector is computed (lines 4 to 8). During the first part of the search (when $\alpha < 0.5$), the distance is the angle to the set of reference vectors (line 5) to promote diversity. During the second part of the search ($\alpha \geqslant 0.5$), the distance is the angle penalized distance defined in Equation (11) (line 7) to enhance both convergence and diversity. Afterward, the candidates are sorted with a lower distance indicating a better search. The sorting is realized per sub-population so that, first, only the lowest distances per sub-population are considered.

5.3. Multi-Task Gaussian Process

The surrogate-model incorporated into AB-MOEA is a Multi-Task Gaussian Process (MTGP) [60]. Relying on a MTGP to model multiple objectives has been realized in [61] to control quality in sheet metal forming. In a traditional regression GP [62], a kernel function is specified to model the covariance between the inputs, thus allowing the model to learn the input-output mapping and to return predictions and predictive uncertainties. In the MTGP, inter-task dependencies are also taken into account in the hope of improving over the case where the tasks are decoupled.

6. Identification of Model Parameters

6.1. Protocol

The two multi-objective optimization problems, 3Obj-3C and 9Obj-3C, are independently solved by running two independent instances of AB-MOEA im-

plemented via the pySBO Python library [63]. For both instances, an initial set of 60 decision vectors obtained via Latin Hypercube Sampling and FE simulations is used to first build the surrogate-model. For each resolution, the time budget for the search is set to 15 days.

6.2. Experimental reference

The experimental research from [64] is used as an experimental reference in this work to validate the results of the 2D plane strain FE orthogonal cutting modeling of Ti6Al4V. The experimental chips were observed with an optical microscope. Globally continuous chips were observed for the three uncut chip thicknesses of h = 0.1 mm, 0.06 mm and 0.04 mm. The chip morphology is shown in Figure 2. The cutting forces are measured in the three directions with a Kistler 9257B dynamometer. The RMS cutting force F_c, RMS feed force F_f, and chip thickness h' (corresponding to variables y_1, y_2 and y_3 in Section 4) observed from the experimental results are given in Table 6.

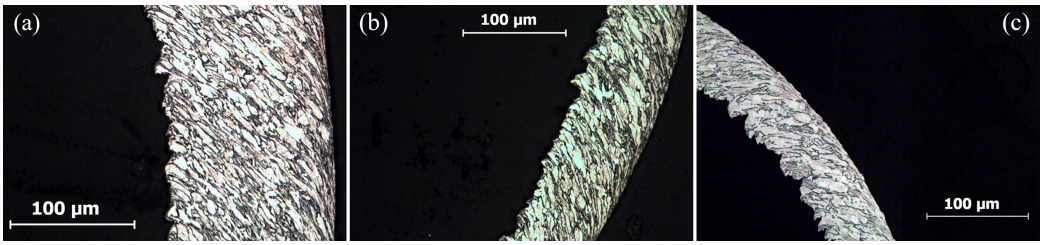

Figure 2: Experimental chips observed with an optical microscope for the uncut chip thickness of (a) h = 0.1 mm, (b) h = 0.06 mm and (c) h = 0.04 mm

Table 6: RMS value of forces and chip thickness measured from experiments for h (mm) = 0.1, 0.06, 0.04 [64]

h (mm)	F_c (N/mm)	F_f (N/mm)	h' (mm)
0.1	173±2	51±1	0.135±0.006
0.06	112±2	45±1	0.080±0.004
0.04	86±2	41±1	0.059±0.005

6.3. Results

6.3.1. Identification of parameter sets

The multi-objective algorithm AB-MOEA outputs a Non-Dominated Set (NDS) of solutions and the associated Non-Dominated Front (NDF) of objective vectors. The solutions composing the NDS are expected to show a trade-off between the different objectives. In machining, cutting and feed forces have usually more importance than chip thickness [65]. Therefore, a higher weight coefficient, 0.35, is chosen for the cutting and feed forces, while it is 0.3 for the chip thickness. For each optimization problem, 3Obj-3C and 9Obj-3C, a unique solution is sampled from the NDS based on the cost function defined in Equation 16:

$$\xi = 0.35 \cdot \left| \frac{F_{c,num} - F_{c,phy}}{F_{c,phy}} \right| + 0.35 \cdot \left| \frac{F_{f,num} - F_{f,phy}}{F_{f,Exp}} \right| + 0.30 \cdot \left| \frac{h'_{num} - h'_{phy}}{h'_{phy}} \right| \quad (16)$$

The two sampled solutions are given in Table 7 along with the corresponding values of the cost function. It can be observed from Table 7 that the cost value is lower for problem 9Obj-3C (0.022) than it is for problem 3Obj-3C (0.025). Consequently, it seems more beneficial to solve the 9-objective problem than its 3-objective counterpart. It is also important to note that the friction coefficient value

is not unique (38% variation). This confirms the identification of both material and friction models in the same procedure is required for the finite element simulation to produce accurate results.

Table 7: Identified parameters sets by the Adaptive Bayesian Multi-Objective Evolutionary Algorithm

Optimization model	B (MPa)	n	m	C	μ	Cost value	Computation time
3Obj-3C	336.1	0.53	0.872	0.0264	0.19	0.025	15 days
9Obj-3C	331.2	0.54	0.714	0.0313	0.28	0.022	15 days

Alternatively to the solutions presented in Table 7, other optimal parameters sets (still obtained by solving the 3Obj-3C and the 9Obj-3C problems) are investigated. The parameters sets generated by solving the 3Obj-3C (resp. 9Obj-3C) problem that predict the quantities of interest within a deviation of 20% are given in Table 8 (resp. Table 9).

Table 8: Other optimal parameters sets generated by solving 3Obj-3C

Parameter	Lower bound	Upper bound
B (MPa)	331.7	352.2
C	0.0264	0.0356
m	0.73	0.87
n	0.46	0.67
μ	0.18	0.28

To monitor the convergence of multi-objective optimization algorithms, the

Table 9: Other optimal parameters sets generated by solving 9Obj-3C

Parameter	Lower bound	Upper bound
B (MPa)	332.4	455.3
C	0.0159	0.0352
m	0.664	0.766
n	0.32	0.57
μ	0.22	0.33

hypervolume is adopted as it is a comprehensive metric. A high hypervolume value indicates a high quality of the best NDF identified so far in terms of convergence, breadth, and uniformity [66]. The hypervolume convergence curves are given in Figure 3 and 4 for the problems 3Obj-3C and 9Obj-3C, respectively. For 3Obj-3C, convergence is reached after 150 iterations of AB-MOEA, while 200 iterations are required for 9Obj-3C. The difference in the number of iterations to convergence is explained by the increase in the difficulty of the 9-objective problem by comparison to the 3-objective one.

6.3.2. Numerical results and validation

The values of the quantities of interest (F_c, F_f and h') simulated with the best parameters sets given in Table 7 are compared with the experimental reference, as well as with numerical results obtained with the parameters set identified via SHPB techniques by Seo et al. [54] (it was found as the best JC set of parameters [18] with the friction coefficient value from [67]). The evaluation of the quantities of interest is conducted at their steady-state to calculate the RMS values. These values and the deviations between simulations and physical experiments are re-

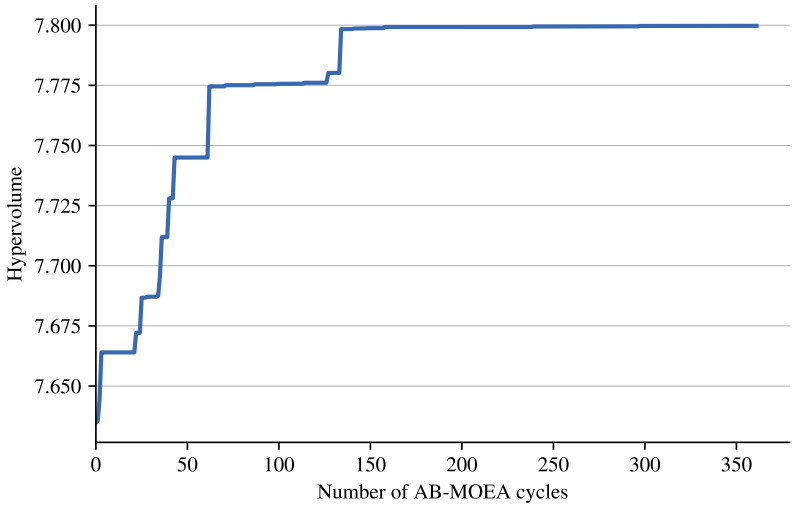

Figure 3: Hypervolume convergence profile for the 3Obj-3C problem

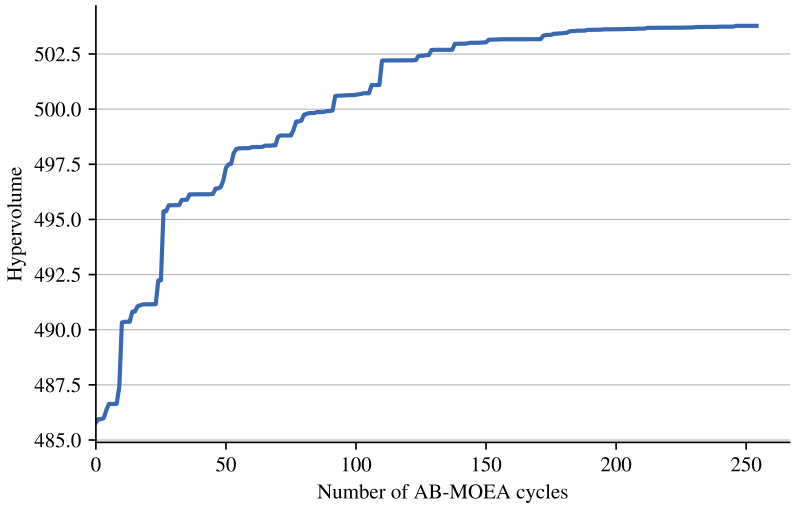

Figure 4: Hypervolume convergence profile for the 9Obj-3C problem

ported in Table 10 for each cutting condition and each optimization problem.

The resolution of both 3Obj-3C and 9Obj-3C problems successfully identifies

Table 10: RMS cutting force F_c, RMS feed force F_f, chip thickness h' and differences with the experimental reference (total difference for the forces Δ_{Force}, total difference for all the quantities of interest Δ_{Total}) for h = 0.1, 0.06, 0.04 mm

h (mm)	Models	F_c (N/mm)	ΔF_c (%)	F_f (N/mm)	ΔF_f (%)	Δ_{Force} (%)	h' (mm)	$\Delta h'$ (%)	Δ_{Total} (%)
0.1	Experiment	173±2	-	51±1	-	-	135±6	-	-
	Seo et al. [54]	177	2	41	22	24	177	27	51
	3Obj-3C	166	4	46	10	14	161	18	32
	9Obj-3C	172	1	51	0	1	166	21	22
0.06	Experiment	112±2	-	45±1	-	-	80±4	-	-
	Seo et al. [54]	120	7	41	9	16	112	33	49
	3Obj-3C	112	0	47	2	2	101	23	25
	9Obj-3C	116	3	46	1	4	107	29	33
0.04	Experiment	86±2	-	41±1	-	-	59±5	-	-
	Seo et al. [54]	92	7	35	15	22	83	41	63
	3Obj-3C	86	0	46	12	12	76	25	37
	9Obj-3C	88	2	41	0	2	78	28	30

599 the JC and Coulomb's models parameters for the simulation of the orthogonal
600 cutting process of Ti6Al4V. Indeed, according to Table 10, the deviation between
601 simulation and physical experiment is reduced in comparison with the JC param-
602 eters set identified by Seo et al. [54] and the friction coefficient from Rech et al.
603 [67]. The total deviation range with the initial parameters is $[49\%; 63\%]$, while
604 $[25\%; 37\%]$ is reached in the case of the 3Obj-3C optimization problem. Solving
605 the 9Obj-3C problem reduces even further the total deviation range to $[22\%; 33\%]$.

606 *6.3.3. Discussion*

607 The relevant parameter sets have been chosen according to the user's interest.
608 Indeed, in this work, more importance is given to forces prediction than to the
609 chip thickness for the selection of the parameters sets. This choice was motivated
610 by the fact that in the machining process, knowledge about the forces is of utmost
611 importance for optimizing the cutting process. A cost function evaluation has been
612 carried out to select the parameter set that provides less deviation of simulated
613 forces with the experimental references. The total difference of simulated results
614 with the experimental results concerning the forces, Δ_{Force}, is given in Table 10.

615 The identified parameters set for JC and Coulomb's friction coefficient by
616 solving the optimization problem 9Obj-3C can accurately predict the cutting and
617 feed forces for all the considered uncut chip thicknesses. Indeed, the forces pre-
618 dicted by the numerical model are in the experimental deviation. However, the
619 parameters set identified by solving the 3Obj-3C problem also show good re-
620 sults by predicting the forces with a difference of 2% for h = 0.06 mm, 12%
621 for h = 0.04 mm, and 14% for h = 0.1 mm.

622 Figures 5 presents an example of temporal evolutions of the forces. As for the
623 other conditions, the steady state is reached after approximately 1.5 ms, then the

quantities of interest are evaluated.

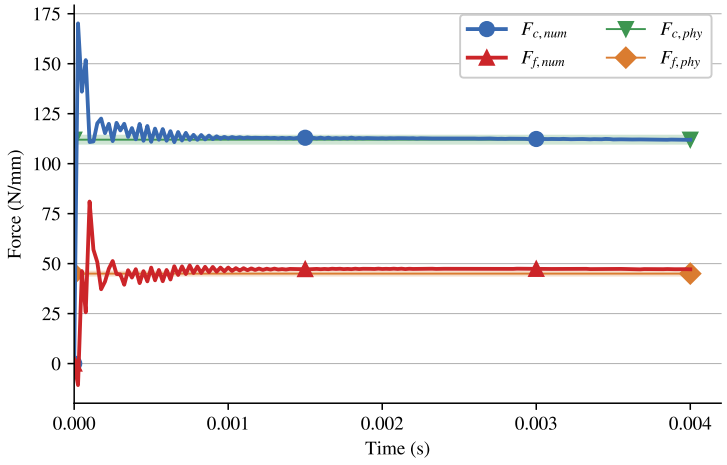

Figure 5: Temporal evolutions of the cutting and feed forces from the FE modeling ($F_{c,num}$ and $F_{f,num}$, respectively) and experimental RMS mean values ($F_{c,phy}$ and $F_{f,phy}$) with their dispersion for h = 0.06 mm and the 3Obj-3C optimization

From the results, it is clear that the simulated forces predicted from the parameters identified by solving the 9Obj-3C problem are slightly better than those predicted by solving the 3Obj-3C problem for all the cutting conditions considered in this work. Nevertheless, both the parameters sets can predict the cutting force within a deviation of less than 4%, a remarkable achievement and a significant improvement compared to the results with the initial parameters from the literature.

The better performance of the 9Obj-3C optimization problem over the 3Obj-3C one is explained by the use of a weighted sum approach to scalarize the objectives in the 3Obj-3C problem formulation. This leads to disadvantages such as the difficulties to set the weight vectors to obtain an optimal solution in the desired region of the objective space or due to the non-convex nature of the objective space,

as highlighted in the literature [68].

6.4. Sensitivity Analysis and Cross-validation

6.4.1. Global sensitivity analysis

In order to evaluate the influence of a model parameter to the quantities of interest, correlation coefficients are computed based on the data set obtained after the optimization runs. A correlation coefficient lies in $[-1; 1]$ and provides information on linear correlation:

- a value in $]0; 1]$ represents a direct correlation;
- a value in $[-1; 0[$ represents an inverse correlation;
- a value equals to 0 indicates no correlation.

The values of the correlation coefficient for every combination of model parameter, quantity of interest and cutting condition are represented via a heat map given in Figure 6.

For the first cutting condition (h = 0.1 mm), parameters B, m and μ show a high influence on the cutting force F_c as demonstrated by the high values of the correlation coefficient (0.40, 0.41 and 0.55, respectively) in Figure 6. The feed force F_f is very sensitive to the parameter μ with a correlation coefficient of 0.81 when $h = 0.1$ mm. For the second cutting condition ($h = 0.06$ mm), both F_c and F_f are very sensitive to μ with correlation coefficients of 0.50 and 0.64, respectively. For the third cutting condition (h = 0.04 mm), inverse correlations are observed between μ and the forces F_c (-0.24) and F_f (-0.22); they are however less strong than for the two other uncut chip thicknesses. There is almost no correlation between parameter C and the results, except for the chip thickness at the two

Figure 6: Correlation between the models parameters and the quantities of interest

largest uncut chip thicknesses. While no clear tendency is highlighted for the other parameters, it is noted that correlations globally differ for the smaller uncut chip thickness. Inverse correlation of the forces with μ and almost no correlation of the chip thickness with parameter n are two examples of differences with the two larger uncut chip thicknesses. This suggests that the reduction of the h/r ratio induces changes in the chip formation process and that, for example, Coulomb's friction should not be used for $h/r < 3$. The second outcome of this part of the study is the highlighting of the high impact of the friction coefficient μ on the quantities of interest. This therefore underlies the importance of considering the friction parameter along with the JC model parameters in the inverse identification problem.

6.4.2. Cross-validation

To evaluate the capacity of the surrogate model to approximate the objective function, a k-fold cross-validation is performed. The performance metric is the Mean Absolute Error (MAE), defined as the average absolute difference between the surrogate predictions and the actual observations:

$$MAE = \frac{1}{n} \sum_{i=1}^{n} \|\boldsymbol{f}(\boldsymbol{x}^{(i)}) - \hat{\boldsymbol{f}}(\boldsymbol{x}^{(i)})\| \tag{17}$$

where n is the number of observations from the data set obtained after the optimization runs, $\boldsymbol{f}$ is the real multi-objective function while $\hat{\boldsymbol{f}}$ is the surrogate prediction.

The k-fold cross-validation consists in splitting the available data set into k sub-sets of equal size. As we choose to set $k = 10$ in this study, each sub-set is composed of 10% of the available data set. For each of the 10 iterations of the cross-validation, the surrogate is trained on all the available data except the sub-set i that is used as test set. After each training, the MAE is computed. At the end of the procedure, the 10 values obtained for the MAE are averaged. The averaged MAE is 0.014 and 0.012 for the 3Obj-3C and the 9Obj-3C problems, respectively. This demonstrates the good approximation performance of the surrogate model. Again, the 9Obj-3C optimization algorithm is slightly better as previously concluded.

7. Conclusions

A surrogate-based multi-objective optimization algorithm was successfully used to determine the parameters values for JC and Coulomb's models for the orthogonal cutting of Ti6Al4V. The multi-objective formulation of the optimization

problem takes into account multiple cutting conditions to optimize the parameters value of both material and friction models together to include the correlation between these aspects.

The Adaptive Bayesian Multi-objective Evolutionary Algorithm (AB-MOEA) handled multiple objectives and computationally intensive objective functions successfully. It was underlined that the proposed formulation of the optimization problem based on the ALE model and solved by AB-MOEA identified the optimal parameters set for the JC and Coulomb's friction models with a total computational time (including the initial data samples simulations) of 17 days with 6 cores of an Intel i7-10700 CPU @2.90 GHz with 16 GiB of Ram.

The major outcomes of this work are the following:

- When solving the 9-objective optimization problem, the identified parameters set led to cutting force and feed force nearly identical to the experimental measurements (the difference is less than 4%) for all the cutting conditions considered in this study.

- When solving the 3-objective optimization problem, the cutting force was also accurately modeled (difference with the experiments of less than 4%), whereas the accuracy was slightly less good for the feed force even though it was still very good (difference in the range of 2% to 12%).

- Both the identified parameters sets significantly improved the prediction accuracy of the chip thickness with differences between 18 % and 29%.

- The results confirmed that the parameters of the material model and of the friction model must be identified together in the same optimization procedure.

The developed ALE FE orthogonal cutting model of Ti6Al4V with the parameters sets identified by solving the multi-objective optimization problems predicted the quantities of interest with high accuracy, which highlights its capability for implementation at the industry level. Furthermore, cross-validation showed the benefits brought by relying on a surrogate-model to solve a computationally expensive multi-objective problem. The automatic parameters identification procedure can be further extended to include more quantities of interest such as chip curvature, temperatures, etc., and also include other cutting conditions such as cutting speeds, tool geometry, etc., to increase the accuracy and expand the range of validity of the models' parameters.

Finally, the introduced method is not tied to the material and friction models, nor to the cutting conditions or any other variable of the cutting process. It was applied in this study to an ALE model and Ti6Al4V, with JC and Coulomb's models, but it is ready for any other applications.

References

[1] Y. Altintas, A. Ber, Manufacturing automation: metal cutting mechanics, machine tool vibrations, and cnc design, Appl. Mech. Rev. 54 (2001) B84–B84.

[2] S. Wang, Z. Tao, D. Wenping, S. Zhanwen, S. To, Analytical modeling and prediction of cutting forces in orthogonal turning: a review, The International Journal of Advanced Manufacturing Technology 119 (2022).

[3] J. Tsekhanov, M. Storchak, Development of analytical model for orthogonal cutting, Production Engineering 9 (2015) 247–255.

[4] A. Markopoulos, Finite Element Method in Machining Processes., ASM, 2012.

[5] P. Arrazola, T. Özel, D. Umbrello, M. Davies, I. Jawahir, Recent advances in modelling of metal machining processes, CIRP Annals - Manufacturing Technology 62 (2013) 695–718.

[6] P. Arrazola, D. Ugarte, J. Montoya, A. Villar, S. Marya, Finite element modeling of chip formation process with abaqus/explicit 6.3 (2005).

[7] D. Furrer, S. Semiatin, Metals Process Simulation, ASM International, 2010.

[8] N. Fang, I. Jawahir, Analytical predictions and experimental validation of cutting force ratio, chip thickness, and chip back-flow angle in restricted contact machining using the universal slip-line model, International Journal of Machine Tools and Manufacture 42 (2002) 681–694.

[9] K. Komvopoulos, S. Erpenbeck, Finite element modeling of orthogonal metal cutting, Journal of Engineering for Industry 113 (1991) 253–267.

[10] S. Melkote, W. Grzesik, J. Outeiro, J. Rech, V. Schulze, H. Attia, P. Arrazola, R. M'Saoubi, C. Saldana, Advances in material and friction data for modelling of metal machining, CIRP Annals - Manufacturing Technology 66 (2017).

[11] F. Ducobu, E. Rivière-Lorphèvre, E. Filippi, Application of the coupled eulerian-lagrangian (cel) method to the modeling of orthogonal cutting, European Journal of Mechanics - A/Solids Volume 59 (2016) 58–66.

[12] F. Ducobu, P.-J. Arrazola, E. Rivière-Lorphèvre, G. O. de Zarate, A. Madariaga, E. Filippi, The cel method as an alternative to the current modelling approaches for ti6al4v orthogonal cutting simulation, Procedia CIRP 58 (2017) 245 – 250. 16th CIRP Conference on Modelling of Machining Operations (16th CIRP CMMO).

[13] T. H. C. Childs, Material property needs in modeling metal machining, Machining Science and Technology 2 (1998) 303–316.

[14] N. Kugalur-Palanisamy, E. Rivière-Lorphèvre, P. J. Arrazola, F. Ducobu, Comparison of johnson-cook and modified johnson-cook material constitutive models and their influence on finite element modelling of ti6al4v orthogonal cutting process, PROCEEDINGS OF THE 22ND INTERNATIONAL ESAFORM CONFERENCE ON MATERIAL FORMING: ESAFORM 2019 (2019).

[15] N. Kugalur-Palanisamy, E. Rivière-Lorphèvre, P. J. Arrazola, F. Ducobu, Influence of coulomb's friction coefficient in finite element modeling of orthogonal cutting of ti6al4v, Key Engineering Materials 926 (2022) 1619.

[16] T. Childs, Friction modelling in metal cutting, Wear 260 (2006) 310–318.

[17] P. J. Arrazola, T. Özel, Investigations on the effects of friction modeling in finite element simulation of machining, International Journal of Mechanical Sciences 52 (2010) 31–42.

[18] F. Ducobu, E. Rivière-Lorphèvre, E. Filippi, On the importance of the choice of the parameters of the johnson-cook constitutive model and their influence

on the results of a ti6al4v orthogonal cutting model, International Journal of Mechanical Sciences 122 (2017) 143–155.

[19] N. Kugalur Palanisamy, E. Rivière Lorphèvre, P.-J. Arrazola, F. Ducobu, Influence of constitutive models and the choice of the parameters on fe simulation of ti6al4v orthogonal cutting process for different uncut chip thicknesses, Journal of Manufacturing and Materials Processing 5 (2021).

[20] H. Chandrasekaran, R. M'Saoubi, H. Chazal, Modelling of material flow stress in chip formation process from orthogonal milling and split hopkinson bar tests, Machining Science and Technology 9 (2005) 131–145.

[21] T. Özel, T. Altan, Determination of workpiece flow stress and friction at the chip–tool contact for high-speed cutting, International Journal of Machine Tools and Manufacture 40 (2000) 133–152.

[22] L. Sterle, F. Pušavec, M. Kalin, Determination of friction coefficient in cutting processes: comparison between open and closed tribometers, Procedia CIRP 82 (2019) 101–106. 17th CIRP Conference on Modelling of Machining Operations (17th CIRP CMMO).

[23] A. Malakizadi, K. Hosseinkhani, E. Mariano, E. Ng, A. D. Prete, L. Nyborg, Influence of friction models on fe simulation results of orthogonal cutting process, The International Journal of Advanced Manufacturing Technology 88 (2017).

[24] G. Globocki Lakic, D. Kramar, J. Kopac, Metal cutting - theory and application, 2014.

[25] G. O. de Zarate, A. Madariaga, P. J. Arrazola, T. H. Childs, A novel methodology to characterize tool-chip contact in metal cutting using partially restricted contact length tools, CIRP Annals 70 (2021) 61–64.

[26] T. Özel, Y. Karpat, Identification of constitutive material model parameters for high-strain rate metal cutting conditions using evolutionary computational algorithms, Materials and Manufacturing Processes 22 (2007) 659–667.

[27] B. Chaparro, S. Thuillier, L. Menezes, P. Manach, J. Fernandes, Material parameters identification: Gradient-based, genetic and hybrid optimization algorithms, Computational Materials Science 44 (2008) 339–346.

[28] A. Milani, W. Dabboussi, J. Nemes, R. Abeyaratne, An improved multi-objective identification of johnson–cook material parameters, International Journal of Impact Engineering 36 (2009) 294–302.

[29] F. Klocke, D. Lung, S. Buchkremer, I. S. Jawahir, From orthogonal cutting experiments towards easy-to-implement and accurate flow stress data, Materials and Manufacturing Processes 28 (2013) 1222–1227.

[30] M. Bäker, A new method to determine material parameters from machining simulations using inverse identification, Procedia CIRP 31 (2015) 399–404. 15th CIRP Conference on Modelling of Machining Operations (15th CMMO).

[31] B. Denkena, T. Grove, M. Dittrich, D. Niederwestberg, M. Lahres, Inverse determination of constitutive equations and cutting force modelling for complex tools using oxley's predictive machining theory, Procedia CIRP 31

(2015) 405–410. 15th CIRP Conference on Modelling of Machining Operations (15th CMMO).

[32] M. Shatla, C. Kerk, T. Altan, Process modeling in machining. part i: determination of flow stress data, International Journal of Machine Tools and Manufacture 41 (2001) 1511–1534.

[33] A. Shrot, M. Baeker, Inverse identification of johnson-cook material parameters from machining simulations, Advanced Materials Research 223 (2011) 277–285.

[34] A. Shrot, M. Bäker, Determination of johnson–cook parameters from machining simulations, Computational Materials Science 52 (2012) 298–304.

[35] P. Bosetti, C. Maximiliano Giorgio Bort, S. Bruschi, Identification of Johnson–Cook and Tresca's Parameters for Numerical Modeling of AISI-304 Machining Processes, Journal of Manufacturing Science and Engineering 135 (2013). 051021.

[36] R. Franchi, A. del prete, D. Umbrello, E. Mariano, Inverse analysis procedure to determine flow stress and friction data for metal cutting finite element modeling, Key Engineering Materials 651-653 (2016) 1345–1350.

[37] T. Bergs, M. Hardt, D. Schraknepper, Inverse material model parameter identification for metal cutting simulations by optimization strategies, MM Science Journal 2019 (2019) 3172–3178.

[38] T. Bergs, M. Hardt, D. Schraknepper, Determination of johnson-cook material model parameters for aisi 1045 from orthogonal cutting tests using the

downhill-simplex algorithm, Procedia Manufacturing 48 (2020) 541–552. 48th SME North American Manufacturing Research Conference, NAMRC 48.

[39] M. Hardt, D. Schraknepper, T. Bergs, Investigations on the application of the downhill-simplex-algorithm to the inverse determination of material model parameters for fe-machining simulations, Simulation Modelling Practice and Theory 107 (2021) 102214.

[40] M. Hardt, D. Jayaramaiah, T. Bergs, On the application of the particle swarm optimization to the inverse determination of material model parameters for cutting simulations, Modelling 2 (2021) 129–148.

[41] M. Hardt, T. Bergs, Considering multiple process observables to determine materialmodel parameters for fe-cutting simulations, The International Journal of Advanced Manufacturing Technology (2021).

[42] N. Kugalur Palanisamy, E. Rivière Lorphèvre, M. Gobert, G. Briffoteaux, D. Tuyttens, P.-J. Arrazola, F. Ducobu, Identification of the parameter values of the constitutive and friction models in machining using ego algorithm: Application to ti6al4v, Metals 12 (2022).

[43] F. Ducobu, N. K. Palanisamy, P.-J. Arrazola, E. Rivière-Lorphèvre, Application of material constitutive and friction models parameters identified with AI and ALE to a CEL orthogonal cutting model, Procedia CIRP 117 (2023) 311–316.

[44] G. R. Johnson, W. H. Cook, A constitutive model and data for metals sub-

jected to large strains, high strain rates and high temperatures, Engineering Fracture Mechanics 21 (1983) 31 – 48.

[45] M. Calamaz, D. Coupard, F. Girot, A new material model for 2d numerical simulation of serrated chip formation when machining titanium alloy ti–6al–4v, International Journal of Machine Tools and Manufacture 48 (2008) 275 – 288.

[46] M. Sima, T. Ozel, Modified material constitutive models for serrated chip formation simulations and experimental validation in machining of titanium alloy ti–6al–4v., International Journalof Machine Tools and Manufacture 50 (2010) 943–960.

[47] A. Markopoulos, N. Vaxevanidis, D. Manolakos, Friction and material modelling in finite element simulation of orthogonal cutting, Tribology in Industry 37 (2015) 440–448.

[48] F. Ducobu, E. Rivière-Lorphèvre, E. Filippi, Numerical contribution to the comprehension of saw-toothed Ti6Al4V chip formation in orthogonal cutting, International Journal of Mechanical Sciences 81 (2014) 77–87.

[49] M. R. Movahhedy, M. S. Gadala, Y. Altintas, Simulation of chip formation in orthogonal metal cutting process: An ale finite element approach, Machining Science and Technology 4 (2000) 15–42.

[50] F. Ducobu, E. Rivière-Lorphèvre, E. Filippi, Mesh influence in orthogonal cutting modelling with the Coupled Eulerian-Lagrangian (CEL) method, European Journal of Mechanics, A/Solids 65 (2017) 324–335.

[51] F. Ducobu, E. Rivière-Lorphèvre, E. Filippi, On the introduction of adaptive mass scaling in a finite element model of ti6al4v orthogonal cutting, Simulation Modelling Practice and Theory 53 (2015) 1–14.

[52] M. Boivineau, C. Cagran, D. Doytier, V. Eyraud, M. H. Nadal, B. Wilthan, G. Pottlacher, Thermophysical properties of solid and liquid ti-6al-4v (TA6v) alloy, International Journal of Thermophysics 27 (2006) 507–529.

[53] D. Leseur, Experimental investigations of material models for ti-6a1-4v and 2024-t3 (1999).

[54] S. Seo, O. Min, H. Yang, Constitutive equation for ti–6al–4v at high temperatures measured using the shpb technique, International Journal of Impact Engineering - INT J IMPACT ENG 31 (2005) 735–754.

[55] M. Emmerich, A. Deutz, A tutorial on multiobjective optimization: fundamentals and evolutionary methods, Natural Computing 17 (2018).

[56] X. Wang, Y. Jin, S. Schmitt, M. Olhofer, An adaptive bayesian approach to surrogate-assisted evolutionary multi-objective optimization, Information Sciences 519 (2020) 317–331.

[57] R. Cheng, Y. Jin, M. Olhofer, B. Sendhoff, A reference vector guided evolutionary algorithm for many-objective optimization, IEEE Transactions on Evolutionary Computation 20 (2016) 773–791.

[58] E. G. Talbi, Metaheuristics: From Design to Implementation, Wiley Series on Parallel and Distributed Computing, Wiley, 2009.

[59] J. A. Cornell, Experiments with Mixtures: Designs, Models, and the Analysis of Mixture Data, John Wiley & Sons, 2002.

[60] E. V. Bonilla, K. Chai, C. Williams, Multi-task gaussian process prediction, in: Advances in Neural Information Processing Systems, volume 20, Curran Associates, Inc., 2008.

[61] W. Xia, H. Yang, X. Liao, J. Zeng, A multi-objective optimization method based on gaussian process simultaneous modeling for quality control in sheet metal forming, The International Journal of Advanced Manufacturing Technology 72 (2014) 1333–1346.

[62] C. E. Rasmussen, Gaussian processes for machine learning, MIT Press, 2006.

[63] G. Briffoteaux, P. Tomenko, F. Geremie, pysbo, a python platform for surrogate-based optimization., 2021. CeCILL licence.

[64] F. Ducobu, E. Rivière-Lorphèvre, E. Filippi, Experimental contribution to the study of the Ti6Al4V chip formation in orthogonal cutting on a milling machine, International Journal of Material Forming 8 (2015) 455–468.

[65] G. Kang, J. Kim, Y. Choi, D. Lee, In-process identification of the cutting force coefficients in milling based on a virtual machining model, International Journal of Precision Engineering and Manufacturing 23 (2022).

[66] E. Zitzler, L. Thiele, Multiobjective evolutionary algorithms: a comparative case study and the strength pareto approach, IEEE transactions on Evolutionary Computation 3 (1999) 257–271.

[67] J. Rech, P. J. Arrazola, C. Claudin, C. Courbon, F. Pusavec, J. Kopac, Characterisation of friction and heat partition coefficients at the tool-work material interface in cutting, CIRP Annals 62 (2013) 79–82.

[68] R. Marler, J. Arora, The weighted sum method for multi-objective optimization: New insights, Structural and Multidisciplinary Optimization 41 (2010) 853–862.